NeuroImage 66 (2013) 449–456

Contents lists available at SciVerse ScienceDirect

NeuroImage

journal homepage: www.elsevier.com/locate/ynimg

Coevolution of brain structures in amnestic mild cognitive impairment

Owen Carmichael [a,*], Donald G. McLaren [b,c,d,e,1], Douglas Tommet [f,2], Dan Mungas [a,3], Richard N. Jones [f,g,4] and for the Alzheimer's Disease Neuroimaging Initiative [5]

[a] Department of Neurology, University of California, Davis, CA, USA
[b] Geriatric Research Education and Clinical Center, ENRM Veterans Hospital, Bedford, MA, USA
[c] Department of Neurology, Massachusetts General Hospital, Charlestown, MA, USA
[d] Athinoula A. Martinos Center for Biomedical Imaging, Massachusetts General Hospital, Charlestown, MA, USA
[e] Harvard Medical School, Boston, MA, USA
[f] Institute for Aging Research, Hebrew SeniorLife, Roslindale, MA, USA
[g] Department of Medicine, Beth Israel Deaconess Medical Center, Harvard Medical School, Boston, MA, USA

ARTICLE INFO

Article history:
Accepted 19 October 2012
Available online 24 October 2012

Keywords:
MRI parcellation
Longitudinal cortical change
Alzheimer's disease
Exploratory factor analysis
Distributed networks

ABSTRACT

Network accounts of the progression of Alzheimer's disease (AD), based on cross-sectional brain imaging observations, postulate that the biological course of the disease is characterized by coordinated spatial patterns of brain change to distributed cognitive networks. This study tests this conjecture by quantifying inter-regional covariance in cortical gray matter atrophy rates in 317 Alzheimer's Disease Neuroimaging Initiative participants who were clinically diagnosed with amnestic mild cognitive impairment at baseline and underwent serial MRI at 6-month intervals over the course of 2 years. A factor analysis model identified five factors (i.e. groupings of regions) that exhibited highly correlated rates of atrophy. Four groupings approximately corresponded to coordinated change within the posterior default mode network, prefrontal cortex, medial temporal lobe, and regions largely spared by the early pathological course of AD (i.e., sensorimotor and occipital cortex), while the fifth grouping represented diffuse, global atrophy. The data-driven observation of "frontal aging" superimposed upon medial temporal atrophy typical of early AD and default mode network changes supports the view that in individuals at high risk of eventual clinical AD, multiple patterns of distributed neuronal death corresponding to multiple biological substrates may be active.

Introduction

Network accounts of brain injury in Alzheimer's disease (AD) are ascendant (Seeley et al., 2009). The spatial progression of the pathological hallmarks of AD has been well understood for many years (Braak and Braak, 1991, 1997), and in vivo studies have noted progressive brain injury, spreading from medial temporal to frontal, lateral temporal, and parietal regions, that partially mirrors this spatial progression (Jack et al., 1997; Thompson et al., 2003). But recent in vivo studies have additionally suggested that the natural course of the disease involves a coordinated attack on a distributed brain network, termed the default-mode network (DMN), that deactivates during execution of many cognitive tasks. Individuals clinically diagnosed with AD, and individuals at elevated risk of clinical AD, show hypometabolism on fluorodeoxyglucose (FDG) positron emission tomography (PET) (Desgranges et al., 1998; Reiman et al., 1996) and deficits on blood oxygenation level dependant (BOLD) functional magnetic resonance imaging (MRI) (Celone et al., 2006; Greicius et al., 2004) within this distributed network, including medial prefrontal, posterior cingulate, and inferior lateral parietal cortical regions. These deficits may mirror injury to the neuronal soma in the same regions, as indicated by T1-weighted structural MRI (Bakkour et al., 2009), as well as degradation of the axonal architecture that connects these regions into distributed networks, as indicated by diffusion MRI (Chua et al., 2008; Greicius et al., 2009). These observations have arisen at a time when traditional imaging-based summary measures of global or focal brain injury have shown limitations in their specificity to clinical and pathological AD, with substantial overlap between groups that do and do not display clinical symptoms and pathological hallmarks (Carmichael et al., 2012; Jagust et al., 2008). The

* Corresponding author at: Center for Neuroscience, 1544 Newton Court, Davis, CA 95618-4859, USA. Fax: +1 530 754 5036.
E-mail addresses: ocarmichael@ucdavis.edu (O. Carmichael), mclaren@nmr.mgh.harvard.edu (D.G. McLaren), DougTommet@hsl.harvard.edu (D. Tommet), jones@hsl.harvard.edu (R.N. Jones).
[1] 149 Thirteenth Street, Charlestown, MA 02129, USA. Fax: +1 617 726 5760.
[2] 1200 Centre Street, Boston, MA 02131, USA. Fax: +1 617 971 5309.
[3] Neurology Department, 4860 Y Street, Suite 3700, Sacramento, CA 95817, USA.
[4] 1200 Centre Street, Boston, MA 02131, USA. Fax: +1 617 971 5309.
[5] Data used in preparation of this article were obtained from the Alzheimer's Disease Neuroimaging Initiative (ADNI) database (adni.loni.ucla.edu). As such, the investigators within the ADNI contributed to the design and implementation of ADNI and/or provided data but did not participate in analysis or writing of this report. A complete listing of ADNI investigators can be found at: http://adni.loni.ucla.edu/wp-content/uploads/how_to_apply/ADNI_Acknowledgement_List.pdf.

1053-8119/$ – see front matter © 2012 Elsevier Inc. All rights reserved.
http://dx.doi.org/10.1016/j.neuroimage.2012.10.029

distributed network account of AD thus has the potential to identify what differentiates AD-related brain changes from those associated with healthy aging in terms of co-occurring change to distributed regions, and thus boost both our understanding of the natural course of the disease and the viability of imaging markers for clinical purposes (Buckner, 2004).

However, the longitudinal imaging studies required to substantiate network accounts of AD have largely been lacking. Multiple imaging sessions per individual are required to show that individuals with clinical or pathological hallmarks of AD display co-occurring, distributed brain changes over time that differ from analogous changes displayed in healthy elders. To date, structural MRI studies supporting the network view have either identified covariances among distributed regions that are related to clinical variables, using cross-sectional imaging data (Bergfield et al., 2010; Brickman et al., 2007; Mechelli et al., 2005; Zhu et al., 2012), or have shown that distributed patterns of deficits at one time point are related to AD-associated clinical outcomes in the future (Bakkour et al., 2009). Structural MRI studies that did include longitudinal imaging, meanwhile, have suggested that trajectories of change in global brain health and focal injury are highly diverse in healthy elders (Raz et al., 2005, 2010; Resnick et al., 2003), are related to concomitant cognitive change (McArdle et al., 2004), and are accelerated on average among those with clinical AD and its prodromes (Driscoll et al., 2009; McDonald et al., 2009). These studies generally did not assess covariance of change across multiple regions in an exhaustive way (Sullivan et al., 2002). Uncertainty about the degree to which distributed, coordinated brain changes over time are detectable on an individual level limit the viability of network hypotheses for characterizing the natural course of the disease.

The purpose of this study is to use longitudinal structural MRI over a 2-year period to identify distributed patterns of coordinated gray matter atrophy in elderly individuals at high risk of clinical AD. In 317 individuals clinically diagnosed with amnestic mild cognitive impairment (aMCI), an AD prodromal condition, we estimated individual rates of change in 34 cortical regions (Desikan et al., 2006) and the hippocampus over a 2 year period. We then used rigorous, data-driven statistical methods to identify groups of regions whose rates of change are highly correlated, as well as determine the number of such groupings that provide the best explanation of longitudinal change.

Materials and methods

Data were obtained from the Alzheimer's Disease Neuroimaging Initiative (ADNI; www.loni.ucla.edu/ADNI). The ADNI was a 5-year study with a primary goal of testing whether serial MRI, positron emission tomography (PET), other biological markers, and clinical and neuropsychological assessment can be combined to measure the progression of amnestic mild cognitive impairment (aMCI) and early Alzheimer's disease (AD). Subjects were recruited from over 50 sites across the U.S. and Canada. The initial goal of ADNI was to recruit 800 adults, ages 55–90, including approximately 200 cognitively normal older individuals to be followed for 3 years, 400 people with aMCI to be followed for 3 years, and 200 people with early AD to be followed for 2 years.

This study includes data from 317 ADNI subjects who were clinically diagnosed with aMCI at baseline and for whom MRI scan data was available from some number of the following examinations: baseline, 6-month follow-up, 12-month follow-up, 18-month follow-up, and 24-month follow-up.

Clinical diagnosis and cognitive evaluation

The clinical assessment of ADNI subjects followed a standardized protocol that was described previously (Petersen et al., 2010). At each evaluation, all participants underwent a standardized clinical evaluation and cognitive tests. Participants were included in the aMCI group if they had a subjective memory complaint, objective memory loss measured by education-adjusted Wechsler Memory Scale-Revised Logical Memory II scores, a Clinical Dementia Rating scale (CDR) global score of 0.5, absence of significant impairment in other cognitive domains, preserved activities of daily living, and an absence of dementia. Exclusion criteria included history of structural brain lesions or head trauma, significant neurological disease other than incipient Alzheimer's disease, use of psychotropic medications that could affect memory, and a Hachinski Ischemic Scale score of 4 or greater. MRI findings that served as exclusionary criteria included major hemispheric infarction, or structural abnormalities that severely distort normal brain anatomy such as tumor or prior resective surgery.

The current study analyzes MRI data from the set of individuals clinically diagnosed with aMCI at baseline.

Brain MRI acquisition

Individuals in the current study had brain MRI data available from some combination of baseline, 6 month, 12 month, 18 month, and 24 month examinations. Acquisition of 1.5 T MRI data at each performance site followed a previously described standardized protocol that was rigorously validated across sites (Jack et al., 2008). The protocol included a high-resolution T1-weighted sagittal volumetric magnetization prepared rapid gradient echo (MP-RAGE) sequence. The ADNI MRI Core optimized the acquisition parameters of these sequences for each make and model of scanner included in the study. Before being allowed to scan ADNI participants, all performance sites were required to pass a strict scanner validation test, including MP-RAGE scans of human subjects and a spherical fluid-filled phantom. Additionally, each scan of ADNI participants included a scan of the phantom, which was required to pass strict validation tests. All vetted raw scan data was transferred to the University of California, San Francisco for automated brain parcellation.

Brain MRI post-processing

MRI scans were parcellated into cortical regions of interest using the longitudinal processing stream in FreeSurfer version 4.3 (surfer.nmr.mgh.harvard.edu). The T1-weighted MR image was first transformed to the Talairach atlas (Talairach and Tournoux, 1988). Next, the main body of white matter was identified by atlas location, intensity, and local neighbors. The variation in intensity across white matter was used to correct bias in the image. The image was then skull stripped, leaving only the brain. Then the image was segmented into subcortical white matter and deep gray matter structures (e.g. hippocampus; Fischl et al., 2002). The remaining voxels were classified as white matter or non-white matter based on intensity and neighbor constraints. For each hemisphere, an initial surface was created along the edge of white matter and refined to follow the white matter/gray matter intensity gradient. This surface was then pushed outward until the intensity gradient between gray matter and cerebrospinal fluid was reached (the pial surface) (Dale et al., 1999; Fischl and Dale, 2000). Next, the sulcal and gyral pattern was aligned to the FreeSurfer average surface (Fischl et al., 1999a, 1999b). This mapping to standard spherical coordinates allowed for automated anatomical parcellation of the cortical surface into 34 gyral regions. Regions included in the cortical parcellation have been described previously (Desikan et al., 2006). The surface parcellation allowed estimation of cortical volumes within each region.

Each tissue segmentation and post-processed cortical parcellation generated by FreeSurfer was assessed at UCSF for global and regional success or failure using a standardized quality control protocol (available from the ADNI web site). MRI scans for individuals who possessed at least three serial MRI scans that passed quality control were re-processed using the longitudinal FreeSurfer workflow (Reuter et al.,

2012). This workflow mirrors the steps that were performed separately on each image in the longitudinal series, but in a combined optimization to encourage longitudinal consistency in tissue segmentation and cortical parcellation (Reuter and Fischl, 2011; Reuter et al., 2010).

There were four quality control outcomes for the UCSF FreeSurfer pipeline based on visual inspection of the parcellated cortical and subcortical region labels superimposed onto anatomical imagery (see http://adni.loni.ucla.edu/wp-content/uploads/2010/12/ADNI_UCSF_Freesurfer-Overview-and-QC.pdf). Scans that were rated as "Pass" showed high-quality parcellation across all cortical and subcortical regions. Scans rated as "Fail" showed a global failure to properly segment the majority of the brain due to gross mis-alignment or poor image quality. Scans rated as "Hippocampus-only" showed a global failure to properly parcellate the cortical surface, but accurate segmentation of the hippocampus. Scans rated as "Partial" showed a failure to accurately parcellate the cortex in one of the following 7 zones: frontal cortex, temporal cortex, insula, parietal cortex, occipital cortex, cerebral white matter, and basal ganglia. For such scans, all regional volumes within the indicated failure zone were excluded from data analysis. The current study includes the 317 individuals who were diagnosed with aMCI at baseline and who had at least one scan from among baseline, 6-month, 12-month, 18-month, and 24-month follow-up examinations that were not rated as "Fail." Among all individuals diagnosed with aMCI at baseline, a total of 1616 MRI scans covering baseline, 6-month, 12-month, 18-month, and 24-month exams were run through the FreeSurfer processing pipeline. Among these, 1158 scans were rated as "Pass," 380 were rated as "Partial," 1 was rated "Hippocampus only," 67 were rated "Fail," and quality control ratings are missing for 10 scans. Among those rated as "Partial," parcellation failures in the temporal, frontal, parietal, insula, occipital, basal ganglia, and cerebral white matter zones were recorded for 145, 347, 347, 86, 388, 67, and 347 scans respectively.

Statistical analysis

The two goals of statistical analysis were to (1) estimate per-individual rates of change in each of the 34 gyral regions and the hippocampus and (2) identify groupings of regions whose rates of change were correlated. As detailed below, we used linear latent growth curve models and exploratory structural equation modeling (ESEM) to achieve these goals.

Pre-processing

For each individual and time point, FreeSurfer provides separate measurements of the volumes of each gyral region in the left and right hemispheres. For each region we calculated the average of corresponding left and right hemisphere volumes, and converted this bilateral region volume to a z-score based on the distribution of volumes from baseline scans. Secondary analyses using just the left or right hemisphere regions were pre-processed the same way.

Individual rates of change

For each bilateral region volume, we used linear latent growth curve models (McArdle, 2009) to estimate individual linear trajectories of regional volume decline. In these models, bilateral region volume was modeled in terms of time from baseline as a fixed linear effect, and inter-individual variability in rate of change was modeled as a random effect. We coded the time of MRI acquisition using a fixed offset from baseline corresponding to 0, 6, 12, 18, and 24-month time points, because visual inspection of the true MRI time point distribution did not suggest substantial or systematic deviation from these standardized times. We also considered so-called "free time" models that allow for modeling of non-linear change trajectories as other ADNI investigators have advocated (Schuff et al., 2012), but visual inspection of estimated trajectories and model fit statistics suggested that linear trajectories provided reasonable fit for most regions (data not shown). Goodness of fit for each bilateral region volume model was evaluated in terms of the standard comparative fit index (CFI) and root mean squared error of approximation (RMSEA) criteria. Bilateral regions for which the estimated inter-individual variance in rate of change was low relative to the standard error of the model (i.e., ratio of variance to standard error less than 2), or for which the mean rate of change was not significantly different from zero, were excluded from subsequent analysis. For all region volume models passing these two tests, change rate estimates for each individual were analyzed to determine inter-regional correlation in change rates using Exploratory Structural Equation Modeling (ESEM; Asparouhov and Muthuen, 2009).

Grouping regions according to covarying rates of change

We then assessed how well the set of change rate estimates is modeled by exploratory factor analysis, a method for accounting for the variance and covariance among a set of variables with a set of latent variables and allowing for each observed variable to account for unique variance. Because exploratory factor analysis models over a range of factor numbers showed inadequate fit (see Results section), we used ESEM to model inter-regional correlation in the residuals of the factor analysis. This allows the model to capture the phenomenon of structured deviations from expected behavior of multiple regions in a local spatial neighborhood, which is not formally allowed in an exploratory factor model. More specifically, any cortical parcellation software is capable of placing boundaries between adjacent regions in incorrect locations. Such measurement error artificially inflates the volume of one of the two regions by a certain amount and artificially deflates the volume of the other region by the same amount. In other words, in this scenario the measurement error in adjacent regions is correlated. Standard factor analysis approaches do not allow such error correlations to be non-zero; ESEM allows us to model these inter-regional error correlations.

To model error correlations between adjacent regions, we started with the average brain surface that FreeSurfer uses to guide the parcellation of cortical surfaces of individual subjects. Each point on the average brain surface is labeled as belonging to one of the 34 cortical regions. For every possible pair of distinct cortical regions, we determined whether there exists at least one pair of adjacent cortical surface points such that one point is labeled as the first region in the pair and the second point is labeled as the second. If any such point pair is found, the pair of regions is labeled as adjacent to one another. Correlations in residuals for all such pairs were modeled in the ESEM model.

ESEM is a generalization of structural equation modeling that allows for the inclusion of fixed or constrained parameters within an exploratory factor analysis framework. In our case, we were interested in a data driven characterization of the shared covariance among change in regional brain volumes, but we wanted to control for residual covariance caused by adjacency of brain regions. We used the adjacencies to identify residual covariance parameters to freely estimate within a general exploratory factor analysis framework. For ESEM models with adequate goodness of fit, factor scores were analyzed to determine which groups of regions changed in a coordinated way. We used the Bayesian Information Criterion (BIC) to determine the number of factors that best explained covariance in longitudinal change.

Secondary analyses

Secondary analyses explored whether bilateral averaging of region volumes may have masked hemisphere-specific patterns of regional change (Derflinger et al., 2011). We ran two analogous ESEM models that included only right hemisphere region change rates, and only left hemisphere region change rates, and compared the region the resulting region groupings with those of the primary model.

Further secondary analyses explored the biological validity of the factor structure of the primary ESEM model. For each individual and factor, standardized factor scores were recorded. These quantify the degree to which the brain regions represented in a given factor atrophied over time to a greater or lesser extent in each individual. Lesser factor scores indicate more loss of brain tissue: the brain regions represented by the factor atrophied at a greater rate over the follow-up period. Greater factor scores indicate greater preservation of the implicated regions. To determine whether greater atrophy in specific factors was associated with greater AD-associated cognitive decline, we used one-tailed *T* tests to compare factor scores between individuals who retained a diagnosis of aMCI throughout the follow-up period ($n=148$) and individuals who converted to a diagnosis of clinical AD at any point in the follow-up period ($n=169$). To determine whether greater burden of AD pathology was associated with greater atrophy to factors suggesting AD-associated neurodegeneration, we identified subgroups of participants who received a lumbar puncture at baseline and had the following three AD pathology markers measured from cerebrospinal fluid using previously described techniques (Trojanowski et al., 2010): amyloid beta 1–42 (Abeta, $n=164$); total tau protein (Tau, $n=161$); and tau protein phosphorylated at threonine 231 (P-tau, $n=165$). We calculated the Pearson correlation between the CSF concentrations of these markers and the factor scores for each of the 5 factors. For Tau and P-tau, negative correlation coefficients mean that greater baseline levels of the CSF protein—suggesting greater burden of AD pathology—were associated with greater amounts of brain atrophy over time. For Abeta, positive correlations mean that lesser baseline levels of the CSF protein—suggesting greater burden of AD pathology—were associated with greater amounts of brain atrophy over time.

Results

General subject characteristics are summarized in Table 1. The group of 317 baseline-aMCI ADNI participants analyzed in the current study is broadly similar to the group of 80 baseline-aMCI ADNI participants who were not included due to a lack of available MRI data. However, participants in the current study were more likely to be Caucasian, and were slightly more likely to be female and left-handed.

Diagnostic summaries of linear latent growth curve models for regional volume change are summarized in Table 2. Model fit was generally excellent, with CFI generally near 1 and RMSEA generally below .03. Relatively poor model fit under these criteria was observed for the following regions: cuneus, frontal pole, insula, lateral occipital cortex, lingual gyrus, parahippocampal gyrus, pericalcarine cortex, and temporal pole. The mean rate of change in all regions was significantly different from zero at the $p<.05$ level. For two regions, the estimate of individual variability in the rate of change was small relative to its standard error: pericalcarine cortex and inferior frontal gyrus - pars orbitalis. Therefore, these latter two regions were excluded from subsequent analyses of inter-regional covariance in rates of change. Summary regional change statistics for all 35 regions are listed in Table 3.

Exploratory factor analysis with 1–11 factors showed inadequate model fit; no model had an observed RMSEA below .05, and all models involving fewer than 8 factors had CFI values lower than .95 (data not shown). A 5-factor ESEM model with pre-specified residual covariances based on adjacency minimized the Bayesian information criterion over all models containing between 1 and 5 factors, and had a CFI of 0.91 and RMSEA of 0.086.

Factor loadings for the 5 factor ESEM model are shown visually in Figs. 1 and 2. The first four factors correspond to co-occurring change in groupings of regions that largely represent: 1. DMN - posterior cingulate, precuneus, inferior parietal, lateral temporo-parietal cortex, and the hippocampus; 2. the frontal lobe; 3. medial temporal cortex, 4. sensory, motor, occipital, and parietal regions including the superior parietal lobule and cuneus. The fifth factor represents diffuse, global change.

The right and left hemisphere ESEM models both identified co-occurring change within frontal, medial temporal, and lateral temporal lobes as in the bilateral model, although lateral temporal and medial temporal changes were joined within the same factor (data not shown). Both models also identified a component of diffuse, global change. Subtle differences emerged between the models in terms of parietal cortex change: while the model for the left hemisphere identified distinct factors corresponding to coordinated parietal and occipital change respectively, the model for the right hemisphere broke up the parietal lobe into two distinct factors.

Those who converted from aMCI to AD showed evidence of much greater atrophy within Factors 1, 2, and 3, which in our schema roughly correspond to the DMN, prefrontal cortex, and medial temporal structures compromised by AD (Table 4). Such differences were much more muted for Factors 4 and 5 ($p>.01$), which correspond to regions generally spared early in the AD course, and non-specific global atrophy. Individuals who had elevated levels of AD pathology burden at baseline (Tau, P-Tau, and ABeta) had greater subsequent atrophy within Factors 1 and 3, which represent the DMN and medial temporal structures (Table 5).

Discussion

The key finding of this study is that, among individuals clinically diagnosed with aMCI at baseline, five distinct spatial patterns of cortical atrophy over a 2-year period were detectable in an unbiased, statistically rigorous analysis. In a well-defined statistical sense, the five spatial patterns provided a superior explanation of longitudinal gray matter atrophy than a single, unifying pattern of global change. The implication is that in the context of prodromal AD, longitudinal brain change may be more accurately modeled in terms of multiple, distinct, spatially distributed atrophy patterns rather than global change or focal lesions to isolated compartments.

Converging evidence from multiple streams of late-life neuroimaging research suggest that the first four spatial patterns may represent

Table 1
Basic characteristics of ADNI participants diagnosed at baseline with aMCI, comparing those who did and did not have MRI data required for inclusion in this study.

	Baseline aMCI with longitudinal MRI		Baseline aMCI without longitudinal MRI
n	317		80
Baseline age	75.4 +/− 7.2		74.8 +/− 8.3
Gender (% male)	63.7%		67.5%
Handedness (% right)	90.5%		93.8%
Race (% Caucasian)	100.0%		67.5%
Years of Education	15.7 +/− 3.0		15.5 +/− 3.3
Baseline MMSE	27.1 +/− 1.7		26.7 +/− 1.9
APOE (% with at least 1 e4 allele)	52.7%		56.3%
Number of MRI at each time point	Baseline	313	
	6-month	300	
	12-month	297	
	18-month	262	
	24-month	215	

Table 2
Fit diagnostics for linear latent growth curve models of brain regional change.

	Mean	S.D.	Range
Mean estimated slope	−0.21	(0.08)	[−0.37,0.03]
Mean estimated slope over standard error [*z*-test]	−11.94	(4.76)	[−21.07,2.23]
CFI	1.00	(0.00)	[0.99,1.00]
RMSEA	0.03	(0.03)	[0.00,0.09]
P-value from model chi-square	0.31	(0.30)	[0.00,0.86]

Table 3
Mean baseline volumes and 2-year changes in volume for the 35 cortical regions. Values are derived from the regional intercepts and slopes output by linear latent growth curve modeling. Mean absolute baseline volume and amount of 2-year change is in units of mm^3. Standardized 2-year change is expressed in standard deviation units: a value of −1 indicates that on average, the region lost 1 standard deviation in volume over 2 years.

Region	Mean volume at baseline	Mean absolute 2-year change	Mean standardized 2-year change
Hippocampus	5808.8	−302.4	−0.29
Banks of superior temporal sulcus	4195.8	−187.9	−0.24
Caudal anterior cingulate	3698.8	−91.7	−0.14
Caudal middle frontal gyrus	10131.5	−356.1	−0.19
Cuneus	5013.4	−37.4	−0.04
Entorhinal cortex	3397.7	−219.7	−0.27
Frontal pole	1282.2	−36.5	−0.13
Fusiform gyrus	16510.5	−804.8	−0.33
Inferior parietal lobule	21962.9	−767	−0.22
Inferior Temporal Gyrus	18768.4	−993.4	−0.31
Insula	11229.7	−344.9	−0.24
Isthmus of cingulate	4012.3	−154.6	−0.24
Lateral occipital	20562.1	−453.3	−0.14
Orbital frontal	12527	−353.1	−0.24
Lingual	11320.8	−203	−0.12
Medial orbital frontal	7572.8	−252.4	−0.25
Middle temporal gyrus	18721.1	−987.6	−0.34
Paracentral lobule	6258.9	−95.5	−0.09
Parahippocampal gyrus	3746.4	−190.9	−0.33
Pars opercularis	7269.4	−232.8	−0.19
Pars orbitalis	4010.4	−105.1	−0.17
Pars triangularis	5911.7	−135.9	−0.12
Pericalcarine	3486	−19.4	−0.03
Postcentral gyrus	15759.2	−166.9	−0.08
Posterior cingulate	5833.4	−196.8	−0.24
Precentral gyrus	21455.6	−519	−0.18
Precuneus	15309.1	−511.3	−0.23
Rostral anterior cingulate	3729	−101.2	−0.15
Rostral middle frontal gyrus	24612.1	−726.3	−0.19
Superior frontal	36011.3	−1219.8	−0.24
Superior parietal lobule	21432.3	−477.4	−0.15
Superior temporal sulcus	19043.8	−747.8	−0.27
Supramarginal gyrus	17413.9	−574.8	−0.23
Temporal pole	3806.8	−234.2	−0.37
Transverse temporal	1703.1	−66.1	−0.2

separable effects of differing biological processes related to aging and AD.

- Factor 1 prominently features posterior cingulate, precuneus, and inferior parietal regions that constitute the posterior section of the so-called default-mode network that is also hypothesized to include medial prefrontal cortex (Buckner, 2004). Evidence from structural and functional MRI, as well as amyloid PET and FDG-PET, suggest that this network may be selectively compromised by the AD pathological process, may disconnect into anterior and posterior subnetworks over the course of the disease, and may be intimately involved in cognitive functions compromised in AD, especially memory (Andrews-Hanna et al., 2007; Buckner et al., 2005; Greicius et al., 2004; Reiman et al., 1996; Sperling et al., 2009).
- Factor 2 mainly represents atrophy of the prefrontal cortex, whose gray matter structures and white matter connections are believed to weaken in a coordinated fashion in so-called "frontal aging" accounts of the mild cognitive deficits, especially to executive control, that have been noted to accompany advancing age in the absence of clinically evident neurodegenerative disease (Buckner, 2004; Pfefferbaum et al., 2005; Raz et al., 1997).
- Factor 3 is dominated by atrophy to the medial temporal lobe, long known to be the earliest locus of neurofibrillary tangle deposition during the pathological course of AD (Braak and Braak, 1991), and long known to exhibit focal atrophy to specific structures that correlate strongly with tangle burden and clinical status (Jack et al., 1992, 1997, 2005).
- Factor 4, meanwhile, is mainly represented by regions such as the sensory strip and occipital cortex that are generally considered to be spared of extensive neuronal loss early in the pathological course of AD.
- Factor 5 represents brain atrophy that is distributed fairly uniformly throughout the cortex.

In summary, the general trend is for the five identified factors to correspond to changes to frontal, medial temporal, posterior default mode network, and AD-spared regions, along with diffuse, global atrophy. The validity of the factors is supported by their plausible associations with concurrent cognitive decline and AD biomarkers: those who declined from aMCI to clinical AD experienced greater atrophy to the factors associated with frontal aging, the posterior default mode network, and AD-associated medial temporal structures. In addition, greater burden of AD pathology at baseline was associated with greater atrophy to the two factors most strongly tied to AD: the posterior default network and the medial temporal lobe. The importance of this finding is that it in a group of individuals assumed to be in the early stage of the AD pathological process, multiple coherent modes of longitudinal brain atrophy may be acting simultaneously, each of which corresponds to a distinct biological substrate. Future work should clarify whether, as appears in the current data, nominally healthy frontal brain aging is superimposed with default mode and medial temporal changes early in the progression of brain changes that eventually culminate in Alzheimer's disease.

Obtaining an adequate representation of longitudinal regional change required a loosening of the EFA assumptions to allow neighboring regions in any individual to deviate from population mean change in a correlated way. We consider two possible scenarios under which such neighborhood correlations would arise. The simplest possibility is that neighborhoods of regions actually do deviate from average behavior in a coordinated way: in any individual, the underlying biological processes leading to greater than expected atrophy to one region may in fact lead to greater than expected atrophy to an adjacent region. Uncertainties in the correspondences between MRI macrostructural region boundaries and the cytoarchitectonic boundaries that define true region-specific change make this possibility especially plausible (Hinds et al., 2008; Yeo et al., 2010a, 2010b). However, another other possibility is that these neighborhood correlations are capturing minor measurement error in the placement of inter-regional boundaries. That is, in the absence of any longitudinal change, any erroneous fluctuation over time in the boundary between one region and its neighbor will necessarily have the dual effect of artificially increasing the volume of one region, and correspondingly lowering the volume of the other, thus causing the two regions to deviate from true zero change in a coordinated way. Further, our simulations suggest that such correlated deviations from expected behavior persist when such erroneous longitudinal boundary fluctuations are superimposed upon true, co-occurring regional volume change (data not shown). Luckily, numerous prior validation studies have suggested that FreeSurfer boundaries agree strongly with ground-truth manual boundary tracings, and that the software produces biologically plausible and self-consistent estimates of longitudinal change (e.g. Han et al., 2006; Jovicich et al., 2006). However, while the sheer magnitude of such region boundary errors is likely to be small, future work should nonetheless more deeply explore the effect that this type of boundary measurement error may have on estimates of inter-regional coordination in volume change.

Longitudinal brain change along the trajectory from normal cognition to clinical AD may follow a complex and nonlinear trajectory that depends strongly on diverse array of factors, including demographic

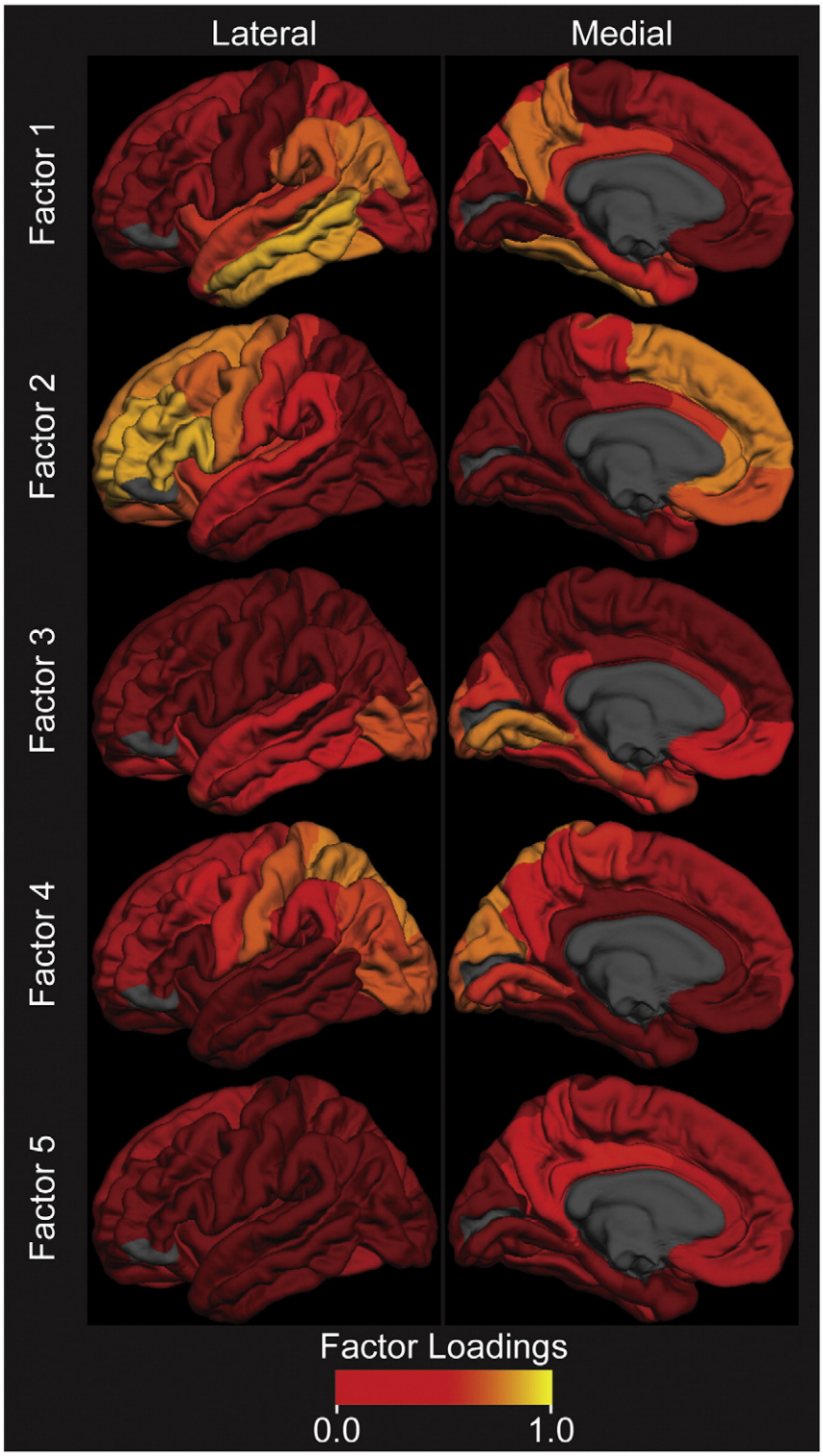

Fig. 1. Visual depiction of the five groupings (factors) of regions that showed high covariance in rates of change according to ESEM modeling. For each factor, regions shown in orange to yellow had strongly co-varying change. The five factors correspond roughly to: 1. posterior default mode network and the hippocampus; 2. the frontal lobe; 3. medial temporal cortex, 4. sensory, motor, occipital, and parietal regions; 5. diffuse, global change.

factors, genetics, and concomitant diseases (Atwood et al., 2004; Buckner, 2004; DeCarli, 2006; Raz et al., 2005; Sowell et al., 2003). The ADNI cohort, by design, represents only a very narrow sampling of those factors. Participants were overwhelmingly Caucasian, highly educated, and were selected to be free of significant concomitant vascular disease (Petersen et al., 2010). The ADNI aMCI group was selected to emphasize a "purely" amnestic sub-type at the expense of other domains of impairment that may fairly commonly co-occur with memory loss in the community (Ganguli et al., 2004). The ADNI normal sub-group was so uniformly healthy that they showed minimal brain changes over 2 years of follow-up; the magnitude of regional atrophy was so small, and inter-regional covariation in change was so minimal, that a factor analysis similar to the one presented here was impossible (data not shown). Thus, it is not clear how the results

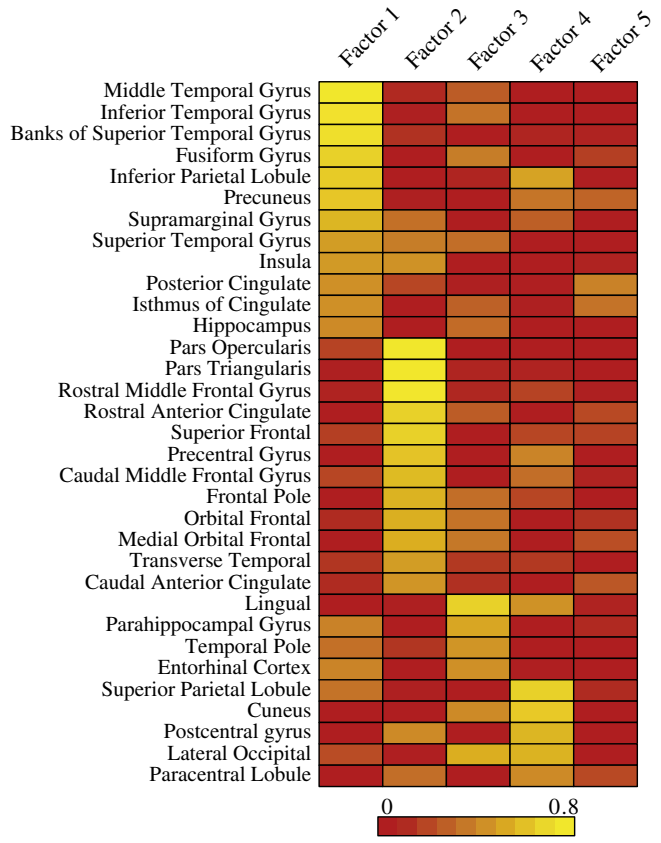

Fig. 2. Listing of region groupings ("factors") that showed coordinated longitudinal change according to factor analysis. Within each factor, regions shown in orange to yellow had strongly co-varying change.

of the current study generalize to the broader population, where brain aging is expected to be more heterogeneous (DeCarli et al., 2005). In addition, aging-associated brain change likely plays out over the course of many years, perhaps decades (Havlik et al., 2002; Korf et al., 2004; Swan et al., 1998), while our study only analyzed change over a narrow 2-year interval. Our observation of multiple biologically patterns of brain change over such a short interval thus motivates future work that applies the statistical methodology to more diverse samples, covering different portions of the spectrum of cognitive decline, imaged over longer intervals.

Each factor includes a minority of additional structures that do not fit cleanly into its overall coherent theme. The hippocampus, for example, had fairly high weightings for both Factor 1 and Factor 3 (.43 vs. .31; see Fig. 2), suggesting that hippocampus change covaried significantly with that of both the medial temporal lobe and the posterior default network. Covariation with the medial temporal lobe is intuitive, but covariation with the default network is plausible as well; the hippocampus and default network exhibit tight functional connectivity during episodic memory task execution, and this connectivity declines during the progression of AD (Greicius et al., 2004). It is plausible that degeneration of such network connectivity is accompanied by coordinated atrophy of the connected regions. Similarly, the lingual gyrus also has non-trivial weightings for both Factor 3 and Factor 4 (.7 vs. .46; see Fig. 2). The association with occipital structures in Factor 4 is biologically plausible. We speculate that the association between lingual gyrus and Factor 3 may be due to difficulty in delineating the boundary between the lingual gyrus and adjacent parahippocampal gyrus. Adequate modeling of longitudinal change in the parahippocampal gyrus was not possible, possibly because this boundary was not delineated with adequate precision. Additionally, systematic error in this boundary could have led parahippocampal atrophy to be reflected in lingual atrophy. In this case, if parahippocampal atrophy were associated with atrophy of other medial temporal structures, atrophy of the lingual gyrus would co-vary with medial temporal atrophy as a by-product.

Table 4
Mean standardized factor scores among individuals who retained a clinical diagnosis of aMCI throughout follow-up (second column), and among those who converted to a clinical diagnosis of AD at any point during follow-up (third column). Lesser scores indicate greater loss of brain tissue within the indicated factor. *P* values for one-tailed t-tests comparing mean factor scores between converter and non-converter groups is also shown (fourth column; $p<.01$ shown in bold).

Factor	Non-converter	Converter	*p*
1	−0.23 (0.01)	−0.30 (0.01)	<**0.0001**
2	−0.17 (0.01)	−0.21 (0.01)	**0.0007**
3	−0.20 (0.01)	−0.26 (0.01)	<**0.0001**
4	−0.14 (0.01)	−0.13 (0.01)	0.9156
5	−0.21 (0.01)	−0.23 (0.01)	0.0112

Table 5
Correlations between standardized factor scores and three cerebrospinal fluid based AD biomarkers (total tau protein, Tau; amyloid beta 1–42, ABeta; and tau protein phosphorylated at threonine 231, P-Tau). Pearson correlation coefficients (ρ) and *p* values for the correlations are shown; correlations with $p<.01$ are shown in bold. For Tau and P-tau, negative correlation coefficients mean that greater baseline levels of the CSF protein—suggesting greater burden of AD pathology—were associated with greater amounts of brain atrophy over time. For Abeta, positive correlations mean that lesser baseline levels of the CSF protein—suggesting greater burden of AD pathology—were associated with greater amounts of brain atrophy over time.

	Factor 1	Factor 2	Factor 3	Factor 4	Factor 5
Tau ρ	**−0.3993**	−0.0115	**−0.1746**	0.1093	0.0992
Tau ρ	**0**	0.885	**0.0268**	0.1677	0.2104
ABeta ρ	**0.29**	0.0585	**0.19**	0.0168	0.1163
Abeta ρ	**0.0002**	0.4568	**0.0148**	0.8314	0.1382
P-tau ρ	**−0.4025**	−0.069	**−0.1761**	0.0685	0.1069
P-tau ρ	**0**	0.3785	**0.0237**	0.3819	0.1718

Funding

Data collection and sharing for this project was funded by the Alzheimer's Disease Neuroimaging Initiative (ADNI) (National Institutes of Health Grant U01 AG024904). ADNI is funded by the National Institute on Aging, the National Institute of Biomedical Imaging and Bioengineering, and through generous contributions from the following: Abbott; Alzheimer's Association; Alzheimer's Drug Discovery Foundation; Amorfix Life Sciences Ltd.; AstraZeneca; Bayer HealthCare; BioClinica, Inc.; Biogen Idec Inc.; Bristol-Myers Squibb Company; Eisai Inc.; Elan Pharmaceuticals Inc.; Eli Lilly and Company; F. Hoffmann-La Roche Ltd and its affiliated company Genentech, Inc.; GE Healthcare; Innogenetics, N.V.; IXICO Ltd.; Janssen Alzheimer Immunotherapy Research & Development, LLC.; Johnson & Johnson Pharmaceutical Research & Development LLC.; Medpace, Inc.; Merck & Co., Inc.; Meso Scale Diagnostics, LLC.; Novartis Pharmaceuticals Corporation; Pfizer Inc.; Servier; Synarc Inc.; and Takeda Pharmaceutical Company. The Canadian Institutes of Health Research is providing funds to support ADNI clinical sites in Canada. Private sector contributions are facilitated by the Foundation for the National Institutes of Health (www.fnih.org). The grantee organization is the Northern California Institute for Research and Education, and the study is coordinated by the Alzheimer's Disease Cooperative Study at the University of California, San Diego. ADNI data are disseminated by the Laboratory for Neuro Imaging at the University of California, Los Angeles. This research was also supported by National Institutes of Health grants AG010129, AG030514, AG030995, AG036694, and AG027171. Drs. Jones was supported in part by the Edward Fein

Foundation (Nevada) and through the generosity of Vicki and Arthur Loring (Massachusetts). The contents do not represent the views of the Dept. of Veterans Affairs, the United States Government, or any other funding entities.

References

Andrews-Hanna, J.R., Snyder, A.Z., Vincent, J.L., et al., 2007. Disruption of large-scale brain systems in advanced aging. Neuron 56, 924–935.

Asparouhov, T., Muthuen, B., 2009. Exploratory structural equation modeling. Struct. Equ. Model. 16, 397–438.

Atwood, L.D., Wolf, P.A., Heard-Costa, N.L., et al., 2004. Genetic variation in white matter hyperintensity volume in the Framingham Study. Stroke 35, 1609–1613.

Bakkour, A., Morris, J.C., Dickerson, B.C., 2009. The cortical signature of prodromal AD. Neurology 72, 1048–1055.

Bergfield, K.L., Hanson, K.D., Chen, K., et al., 2010. Age-related networks of regional covariance in MRI gray matter: reproducible multivariate patterns in healthy aging. Neuroimage 49, 1750–1759.

Braak, H., Braak, E., 1991. Neuropathological stageing of Alzheimer-related changes. Acta Neuropathol. 82, 239–259.

Braak, H., Braak, E., 1997. Staging of Alzheimer-related cortical destruction. Int. Psychogeriatr. 9 (Suppl. 1), 257–261 (discussion 269–272).

Brickman, A.M., Habeck, C., Zarahn, E., Flynn, J., Stern, Y., 2007. Structural MRI covariance patterns associated with normal aging and neuropsychological functioning. Neurobiol. Aging 28, 284–295.

Buckner, R.L., 2004. Memory and executive function in aging and AD: multiple factors that cause decline and reserve factors that compensate. Neuron 44, 195–208.

Buckner, R.L., Snyder, A.Z., Shannon, B.J., et al., 2005. Molecular, structural, and functional characterization of Alzheimer's disease: evidence for a relationship between default activity, amyloid, and memory. J. Neurosci. 25, 7709–7717.

Carmichael, O., Mungas, D., Beckett, L., et al., 2012. MRI predictors of cognitive change in a diverse and carefully characterized elderly population. Neurobiol. Aging 33 (1), 83–95 (Jan).

Celone, K.A., Calhoun, V.D., Dickerson, B.C., et al., 2006. Alterations in memory networks in mild cognitive impairment and Alzheimer's disease: an independent component analysis. J. Neurosci. 26, 10222–10231.

Chua, T.C., Wen, W., Slavin, M.J., Sachdev, P.S., 2008. Diffusion tensor imaging in mild cognitive impairment and Alzheimer's disease: a review. Curr. Opin. Neurol. 21, 83–92. http://dx.doi.org/10.1097/WCO.1090b1013e3282f4594b.

Dale, A.M., Fischl, B., Sereno, M.I., 1999. Cortical surface-based analysis. I. Segmentation and surface reconstruction. Neuroimage 9, 179–194.

DeCarli, C.S., 2006. When two are worse than one: stroke and Alzheimer disease. Neurology 67, 1326–1327.

DeCarli, C., Massaro, J., Harvey, D., et al., 2005. Measures of brain morphology and infarction in the framingham heart study: establishing what is normal. Neurobiol. Aging 26, 491–510.

Derflinger, S., Sorg, C., Gaser, C., et al., 2011. Grey-matter atrophy in Alzheimer's disease is asymmetric but not lateralized. J. Alzheimers Dis. 25, 347–357.

Desgranges, B., Baron, J.C., de la Sayette, V., et al., 1998. The neural substrates of memory systems impairment in Alzheimer's disease. A PET study of resting brain glucose utilization. Brain 121, 611–631.

Desikan, R.S., Segonne, F., Fischl, B., et al., 2006. An automated labeling system for subdividing the human cerebral cortex on MRI scans into gyral based regions of interest. Neuroimage 31, 968–980.

Driscoll, I., Davatzikos, C., An, Y., et al., 2009. Longitudinal pattern of regional brain volume change differentiates normal aging from MCI. Neurology 72, 1906–1913.

Fischl, B., Dale, A.M., 2000. Measuring the thickness of the human cerebral cortex from magnetic resonance images. Proc. Natl. Acad. Sci. U. S. A. 97, 11050–11055.

Fischl, B., Sereno, M.I., Dale, A.M., 1999a. Cortical surface-based analysis. II. Inflation, flattening, and a surface-based coordinate system. Neuroimage 9, 195–207.

Fischl, B., Sereno, M.I., Tootell, R.B., Dale, A.M., 1999b. High-resolution intersubject averaging and a coordinate system for the cortical surface. Hum. Brain Mapp. 8, 272–284.

Fischl, B., Salat, D.H., Busa, E., et al., 2002. Whole brain segmentation: automated labeling of neuroanatomical structures in the human brain. Neuron 33, 341–355.

Ganguli, M., Dodge, H.H., Shen, C., DeKosky, S.T., 2004. Mild cognitive impairment, amnestic type: an epidemiologic study. Neurology 63, 115–121.

Greicius, M.D., Srivastava, G., Reiss, A.L., Menon, V., 2004. Default-mode network activity distinguishes Alzheimer's disease from healthy aging: evidence from functional MRI. Proc. Natl. Acad. Sci. U. S. A. 101, 4637–4642.

Greicius, M.D., Supekar, K., Menon, V., Dougherty, R.F., 2009. Resting-state functional connectivity reflects structural connectivity in the default mode network. Cereb. Cortex 19, 72–78.

Han, X., Jovicich, J., Salat, D., et al., 2006. Reliability of MRI-derived measurements of human cerebral cortical thickness: the effects of field strength, scanner upgrade and manufacturer. Neuroimage 32, 180–194.

Havlik, R.J., Foley, D.J., Sayer, B., Masaki, K., White, L., Launer, L.J., 2002. Variability in midlife systolic blood pressure is related to late-life brain white matter lesions. Stroke 33, 26–30.

Hinds, O.P., Rajendran, N., Polimeni, J.R., et al., 2008. Accurate prediction of V1 location from cortical folds in a surface coordinate system. Neuroimage 39, 1585–1599.

Jack Jr., C.R., Petersen, R.C., O'Brien, P.C., Tangalos, E.G., 1992. MR-based hippocampal volumetry in the diagnosis of Alzheimer's disease. Neurology 42, 183–188.

Jack Jr., C.R., Petersen, R.C., Xu, Y.C., et al., 1997. Medial temporal atrophy on MRI in normal aging and very mild Alzheimer's disease. Neurology 49, 786–794.

Jack Jr., C.R., Shiung, M.M., Weigand, S.D., et al., 2005. Brain atrophy rates predict subsequent clinical conversion in normal elderly and amnestic MCI. Neurology 65, 1227–1231.

Jack Jr., C.R., Bernstein, M.A., Fox, N.C., et al., 2008. The Alzheimer's Disease Neuroimaging Initiative (ADNI): MRI methods. J. Magn. Reson. Imaging 27, 685–691.

Jagust, W.J., Zheng, L., Harvey, D.J., et al., 2008. Neuropathological basis of magnetic resonance images in aging and dementia. Ann. Neurol. 63, 72–80.

Jovicich, J., Czanner, S., Greve, D., et al., 2006. Reliability in multi-site structural MRI studies: effects of gradient non-linearity correction on phantom and human data. Neuroimage 30, 436–443.

Korf, E.S.C., White, L.R., Scheltens, P., Launer, L.J., 2004. Midlife blood pressure and the risk of hippocampal atrophy. Hypertension 44, 29–34.

McArdle, J.J., 2009. Latent variable modeling of differences and changes with longitudinal data. Annu. Rev. Psychol. 60, 577–605.

McArdle, J.J., Hamgami, F., Jones, K., et al., 2004. Structural modeling of dynamic changes in memory and brain structure using longitudinal data from the normative aging study. J. Gerontol. B Psychol. Sci. Soc. Sci. 59, P294–P304.

McDonald, C.R., McEvoy, L.K., Gharapetian, L., et al., 2009. Regional rates of neocortical atrophy from normal aging to early Alzheimer disease. Neurology 73, 457–465.

Mechelli, A., Friston, K.J., Frackowiak, R.S., Price, C.J., 2005. Structural covariance in the human cortex. J. Neurosci. 25, 8303–8310.

Petersen, R.C., Aisen, P.S., Beckett, L.A., et al., 2010. Alzheimer's Disease Neuroimaging Initiative (ADNI): clinical characterization. Neurology 74, 201–209.

Pfefferbaum, A., Adalsteinsson, E., Sullivan, E.V., 2005. Frontal circuitry degradation marks healthy adult aging: evidence from diffusion tensor imaging. Neuroimage 26, 891–899.

Raz, N., Gunning, F.M., Head, D., et al., 1997. Selective aging of the human cerebral cortex observed in vivo: differential vulnerability of the prefrontal gray matter. Cereb. Cortex 7, 268–282.

Raz, N., Lindenberger, U., Rodrigue, K.M., et al., 2005. Regional brain changes in aging healthy adults: general trends, individual differences and modifiers. Cereb. Cortex 15, 1676–1689.

Raz, N., Ghisletta, P., Rodrigue, K.M., Kennedy, K.M., Lindenberger, U., 2010. Trajectories of brain aging in middle-aged and older adults: regional and individual differences. Neuroimage 51, 501–511.

Reiman, E.M., Caselli, R.J., Yun, L.S., et al., 1996. Preclinical evidence of Alzheimer's disease in persons homozygous for the epsilon 4 allele for apolipoprotein E. N. Engl. J. Med. 334, 752–758.

Resnick, S.M., Pham, D.L., Kraut, M.A., Zonderman, A.B., Davatzikos, C., 2003. Longitudinal magnetic resonance imaging studies of older adults: a shrinking brain. J. Neurosci. 23, 3295–3301.

Reuter, M., Fischl, B., 2011. Avoiding asymmetry-induced bias in longitudinal image processing. Neuroimage 57, 19–21.

Reuter, M., Rosas, H.D., Fischl, B., 2010. Highly accurate inverse consistent registration: a robust approach. Neuroimage 53, 1181–1196.

Reuter, M., Schmansky, N.J., Rosas, H.D., Fischl, B., 2012. Within-subject template estimation for unbiased longitudinal image analysis. NeuroImage 61 (4), 1402–1418 (July 16).

Schuff, N., Tosun, D., Insel, P.S., et al., 2012. Nonlinear time course of brain volume loss in cognitively normal and impaired elders. Neurobiol. Aging 33, 845–855.

Seeley, W.W., Crawford, R.K., Zhou, J., Miller, B.L., Greicius, M.D., 2009. Neurodegenerative diseases target large-scale human brain networks. Neuron 62, 42–52.

Sowell, E.R., Peterson, B.S., Thompson, P.M., Welcome, S.E., Henkenius, A.L., Toga, A.W., 2003. Mapping cortical change across the human life span. Nat. Neurosci. 6, 309–315.

Sperling, R.A., Laviolette, P.S., O'Keefe, K., et al., 2009. Amyloid deposition is associated with impaired default network function in older persons without dementia. Neuron 63, 178–188.

Sullivan, E.V., Pfefferbaum, A., Adalsteinsson, E., Swan, G.E., Carmelli, D., 2002. Differential rates of regional brain change in callosal and ventricular size: a 4-year longitudinal MRI study of elderly men. Cereb. Cortex 12, 438–445.

Swan, G.E., DeCarli, C., Miller, B.L., et al., 1998. Association of midlife blood pressure to late-life cognitive decline and brain morphology. Neurology 51, 986–993.

Talairach, J., Tournoux, P., 1988. Co-planar stereotaxic atlas of the human brain. 3-Dimensional proportional system: an approach to cerebral imaging. Thieme.

Thompson, P.M., Hayashi, K.M., de Zubicaray, G., et al., 2003. Dynamics of gray matter loss in Alzheimer's disease. J. Neurosci. 23, 994–1005.

Trojanowski, J.Q., Vandeerstichele, H., Korecka, M., Clark, C.M., Aisen, P.S., Petersen, R.C., Blennow, K., Soares, H., Simon, A., Lewczuk, P., Dean, R., Siemers, E., Potter, W.Z., Weiner, M.W., Jack Jr., C.R., Jagust, W., Toga, A.W., Lee, V.M.-Y., Shaw, L.M., 2010. Update on the biomarker core of the Alzheimer's Disease Neuroimaging Initiative subjects. Alzheimers Dement. 6 (3), 230–238 (May).

Yeo, B.T., Sabuncu, M.R., Vercauteren, T., Ayache, N., Fischl, B., Golland, P., 2010a. Spherical demons: fast diffeomorphic landmark-free surface registration. IEEE Trans. Med. Imaging 29, 650–668.

Yeo, B.T., Sabuncu, M.R., Vercauteren, T., et al., 2010b. Learning task-optimal registration cost functions for localizing cytoarchitecture and function in the cerebral cortex. IEEE Trans. Med. Imaging 29, 1424–1441.

Zhu, W., Wen, W., He, Y., Xia, A., Anstey, K.J., Sachdev, P., 2012. Changing topological patterns in normal aging using large-scale structural networks. Neurobiol. Aging. Neurobiol. Aging 33 (5), 899–913.